Evolution of spall-damage in iron caused by repeated plate impacts: Ultrasonic evaluation

N. Nishimura[a, *]

nisimura@meijo-u.ac.jp

K. Fujimoto[b]

Y. Ogi[b]

T. Ito[c]

[a]Department of Vehicle and Mechanical Engineering, Meijo University, 1-501 Shiogamaguchi, Tempaku-ku, Nagoya 468-8502, Japan

[b]Division of Vehicle and Mechanical Engineering, Graduate School of Science and Technology, Meijo University, 1-501 Shiogamaguchi, Tempaku-ku, Nagoya 468-8502, Japan

[c]Department of Mechanical Engineering, Nagoya Institute of Technology, Gokiso-cho, Showa-ku, 468-8555 Nagoya, Japan

*Corresponding author.

Abstract

This paper focuses on the developed of spall-damage that occurs in pure iron as a result of repeated impact. The employed low-frequency scanning acoustic microscopy (LF-SAM) observations combined with the measurements of ultrasonic wave velocity, attenuation, backscattering intensity and amplitude spectrum of the reflected wave, enabled us to provide a nondestructive evaluation. The spall-damage distribution was analyzed in the C-scan images, and we found the spall-damage increase with impact stress when the latter exceeds the characteristic spall-threshold stress. Moreover, we recorded the decreased sound velocity, amplitude ratio, and the increase of backscattering intensity, significant attenuation (the high frequency component of the reflected wave) for enhanced impact stress. It was also demonstrated that the tiny cracks generated in iron develop significantly during subsequent impacts either with lower or higher impact stress. Since the presented results concern for the first time the multiple-impact experiments, we contend that the applied ultrasonic investigations constitute the effective method of nondestructive spall-damage evaluation.

Keywords: Spall damage; Repeated plate impact test; Stress wave; Ultrasonic inspection; Non-destructive evaluation

1 Introduction

It is already widely recognized that the pulses of significant tensile stress-produced by high-velocity impacts of solid-particles on a metallic surface result in spall-damage of the tested material, associated with nucleation of micro-voids or micro-cracks are nucleated in the body of solid. These imperfections, although sizable, are hard to detect and measure, since they are formed mainly in subsurface region. Therefore, the conventional examination of spall-damage usually involves microscopic observations of a set of cross-sections through the sample in a damaged material region [1–3]. Such a tedious, destructive, costly, and yet inaccurate method certainly discourages researchers to thoroughly examine this interesting phenomenon, while it appears also unsuitable for the ‘in-service inspection’ of structural components. In a consequence, the indicated shortcomings prompted us to search for a nondestructive technique that provides information about the development of the impact-induced spall damage, while applicable to the commercial structures. The ultrasonic examination of spall-damage appears as a proper approach to address this technologically and scientifically important problem.

Indeed, the spall damage severity and its localization can be assessed with the ultrasonic method (C- and B-scan images) capable of detecting defects and dissimilar inclusions generated during impact testing. The depth-distribution of defects in a plane parallel to the impacted surface has been already demonstrated [4–6], while the method we present that includes pulse-echo measurements of ultrasonic wave velocity, attenuation (amplitude changes from B2 to B1 echo) and recording of wave intensity scattered on defects [7], proves usefulness of C- and B-scans for multiple impact experiments. The advantages of the ultrasonic measurements as the convenient, precise and efficient approach to evaluation of spall damage in aluminum and medium carbon steel during consecutive impacts had already been demonstrated [8,9].

This paper, however, contrasts the previously published results as it focuses on the evaluation of the spall-damage produced exclusively during repeated impacting of commercially pure iron. Moreover, additional ultrasonic

parameter, the amplitude spectrum of backwall echo (B1), was considered for quantitative ultrasonic evaluation.

2 Spallation process under plate impact test

The spall damage that appears either as micro-voids or micro-cracks nucleated within a target plate by tri-axial tensile stress pulse, is generated by the plate impact test. When a target plate is impacted by a flyer plate, the compressive stress waves generated in both plates travel toward the free surfaces, where they are reflected with the reversed phase [8]. The reflected tensile waves propagate towards the impacted surface and superimpose with the initial 'compressive waves' (rarefaction). When rarefaction waves within target plate propagated from impacted and free surfaces superimpose, a tensile stress pulse is generated, which amplitude and duration considerably affects a development of spall damage [1,2]. In the case when the impact stress is higher than the threshold spall stress of the solid, and its duration is long enough to create tensile failure of material, the spall damage is nucleated in the narrow range called the 'spall plane'. The latter gives origin to further formation of macro-cracks.

3 Experimental methods

3.1 Plate impact tests

Target plates made of commercially pure iron (Daido steel Co., Ltd., ME1, purely 99.5%) was impacted repeatedly by flyer plates of the same material (the detailed characteristics are given in Table 1). The detailed listing of the conditions of the experiments carried out on different specimens is provided in Table 2. The dimensions of the used materials and schematic of the experimental setup is illustrated in Fig. 1. The parallel orientation of the target and flyer plates was secured within our experiments (the deviation should not exceed 1 mrad as stated in [10]).

Table 1 Material characteristics of the commercially pure iron.

Chemical composition (mass%)	C	Si	Mn	P	S		
	0.02	0.2	0.2	0.02	0.02		
Material parameters	Density ρ [kg/m^3]	Poisson's ratio ν	Young's modulus E [GPa]	Bulk modulus K [GPa]	Shear modulus G [GPa]	Elastic wave velocity C_e [m/s]	Plastic wave velocity C_p [m/s]
	7850	0.29	212	166	82	5930	4600

Table 2 The detailed listing of the test conditions carried out on commercially pure iron specimens and the occurrence of spall damage after the first impact detected by SLFAM-technique. The symbols ○ and × stand for distinguished and non- identified spall damage, respectively.

Specimen No.	Impact velocity V [m/s]	Impact stress σ [GPa]	Spall damage
N5	96	2.2	×
N6	73	1.7	×
N7	138	3.2	○
N14	86	2.0	×
N18	196	4.6	○

Specimen No.	First impact		Second impact		Third impact	
	Impact velocity V [m/s]	Impact stress σ [GPa]	Impact velocity V [m/s]	Impact stress σ [GPa]	Impact velocity V [m/s]	Impact stress σ [GPa]
N1	151	3.5	78	1.8	150	3.5
N2	158	3.7	198	4.6	–	–
N4	119	2.8	165	3.8	209	4.9

N10	99	2.3	83	1.9	83	1.9
N16	111	2.6	121	2.8	–	–
N17	146	3.4	102	2.4	96	2.2

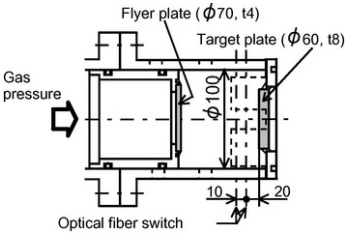

Fig. 1 Location of the target, flyer and the 'velocity measurement unit' denoted in the schematic of the experimental setup. The exact dimensions used in our experiments are indicated in the figure.

The flyer plate bonded to the polymer sabot was accelerated by a single stage gas-gun, while the target plate was bonded to the plastic stage fastened to the target holder and velocity measurement unit (details in Fig. 1). The flyer impact velocity was measured by the optical fiber switches located 20 and 30 mm away from the target plate. The special recovery chamber has been constructed to recuperate the target plate for further tests [8]. After each impact event, the front and rear surfaces of the target plate were polished with a grinder or the #1500 emery paper. At maximum of three repeated impacts were applied to one given target plate with different impact velocities (see Table 2).

When the target and flyer are made of the same material, the compressive stress σ induced right after the collision can be obtained from the relationship [8,11,12]:

$$\sigma = \frac{1}{2}\rho CV \quad ,C = \sqrt{\frac{1}{\rho}\left(K + \frac{4}{3}G\right)}, \tag{1}$$

where ρ, C, V, K and G are the density, the bulk (elastic) wave velocity, the velocity of the flyer, the bulk elastic modulus and the shear elastic modulus of an investigated material, respectively.

3.2 C-scan imaging

In order to characterize the spall-damage generation and distribution induced in the target plate, we used the scanning low frequency acoustic microscopy (SLFAM, Olympus UH Pulse-100 – the schematic given in Fig. 2, see also Refs. [4,6,13]). UH microscope employed the frequency range, gate width and memory size of 5-200 MHz, 20 ns-1 μs and 640 × 512 (8bit), respectively. The spall damage was examined by ultrasonic C- or B-scan images to visualize void/crack distributions, *i.e.*, C-scan in a plane parallel to impact plane at arbitrary depth, B-scan in a plane perpendicular to impact plane. The scanning acoustic images were obtained by detection of the amplitude of the longitudinal wave reflected from the elemental area of the specific defects such as inclusions, voids or cracks. The signal intensity recorded at each point was mapped as a set of spots of variable brightness (*e.g.*, Fig. 4 in the Results chapter). The following parameters were used in the experiments: the central frequency of 30 MHz, beam diameter at focus equal 0.28 mm and focal length (in water) of 25.4 mm [14] were achieved with the PolyVinylidene DiFluoride (PVDF) point-focus transducer, similarly as in previous work [8]. A PVDF transducer is free from the noise owing to the reverberation at the lens surface in the conventional transducer, therefore voids or cracks in arbitrary depth are properly revealed (see Ref. [8]).

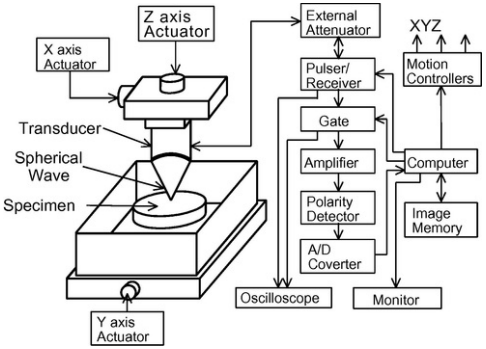

Fig. 2 The clarification of our acoustic microscopy provided in a graphical form. To suppress the ringing of the reflected wave, an external attenuator was added to the measuring circuit, while the additional oscilloscope was used to detect the acoustic wave reflected from the damaged zone.

Specimens were inspected by SLFAM before the initial impact in order to confirm the absence of pre-existing voids or cracks. C-scan images were acquired at the 2.0, 2.5, 3.0, 3.5, 3.75 and 4.0 mm depths from the impact surface, while B-scan images were taken at the central cross-section of the target plate. The gate width was fixed at 30 ns, which corresponds to the thickness of approx. 90 μm, for the commercially pure iron.

3.3 Quantitative evaluation of spall damage

The spall damage evolution was determined from the wave intensity backscattered at defects, using the amplitude spectrum of the backwall echo (B1) in addition to the former parameters (time-of-flight, longitudinal wave velocity. The backwall echoes (B1 and B2) of the target plates and the backscattering intensity scattered at the spall damage) [8,9] are defined in Fig. 3. The used digital ultrasonic measurement system [15] was composed of ultrasonic pulser/receiver, A/D converter board and personal computer. The longitudinal wave transducer (frequency of 10 MHz, diameter 6.4 mm) made it possible to record the backscattering echoes at different locations, namely at the center and 10 mm both sides away of it. The measurements were performed before, and right after the impact test.

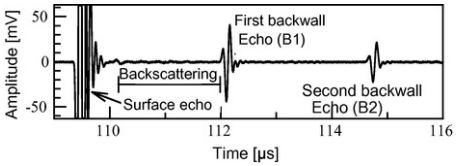

Fig. 3 The typical waveform recorded using the ultrasonic measurement (specimen No. N4). The obtained data spanning from surface echo to second backwall echo (B2) were used for analyzing the ultrasonic variables.

The recorded waveforms depicted in Fig. 3 (see also Ref. [8]) provide the data concerning ultrasonic velocity and attenuation as amplitude ratio of B2 to B1 echo. The backscattering intensity, characterized by the non-dimensional frequency-dependent value N reads [8]:

$$N = \int_{f_1}^{f_2} B(f)df / \int_{f_1}^{f_2} U(f)df, \quad \textbf{(2)}$$

where $B(f)$ defines the amplitude spectrum of the backscattering wave, $U(f)$ denotes the surface echo, f_1 and f_2 are the lower and upper limit of the frequency f. The backscattering wave was recorded from the depth of 3 mm below the impact surface and terminated at the back surface (Fig. 3). The frequency range spanned from 3 to 14 MHz which secured higher amplitude. The spectrum of the reflected waves was evaluated by the ratio of the amplitude for the impacted specimen and the non-impacted one, while the target plates were examined after consecutive impacts. We determined ultrasonic velocity, attenuation, backscattering intensity and amplitude spectrum together with C- and B-scan imaging. After the final ultrasonic measurement, the cross-sections of the target plate were examined by the optical microscopy.

4 Results and discussion

4.1 Spall damage generated by the initial impact

The threshold stress that results in generating of spall damage in the commercially pure iron was evaluated. It was found that the impact stress should be no less than 2.3 GPa, while the medium carbon steel requires 2.6 GPa

to initiate destruction of material [8]. The detailed account for the impact test conditions and the cases when flaws were detected by the SLFAM are listed in Table 2. The evaluation of the impact stress pertinent to our study was accomplished using the general formula (Eq. (1)) with the proper material's parameters (Table 1) and flyer's velocities (Table 2).

4.2 Changes in cracks distribution during repeated plate impacts

The C-scan images (Figs. 4–6) reveal spall damage created in the commercially pure iron after the first (a), second (b) and third (c) impact. These images were taken in the determined region of the target plate with the same imaging conditions. The white spots caused by reflected signal indicate the defects. In the repeated plate impact tests, we applied different sequences of impact stresses to selected specimens (see the details in Table 2) in order to establish relationship between the stress level sequence of impacts and the resulting damage. Our experimental results are completed by optical microscopy observation of the spall damage (the example given in Fig. 7). Thus the change in these images shows the damage evolution.

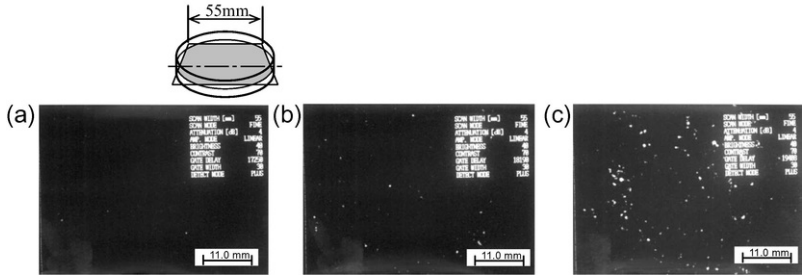

Fig. 4 The variation of spall-damage in commercially pure iron (sample No. N4) induced by consecutive impacts during repeated testing with the second impact stress (3.8 GPa) higher than the first one (2.8 GPa). The C-scan images taken at the depth of 3.5 mm below the impact surface illustrate the scenario after the first (a), second (b) and third (c) impact, for which the applied impact stress equaled 2.8, 3.8 and 4.9 GPa, respectively.

Fig. 5 The variation of spall-damage in commercially pure iron (sample No. N1) induced by consecutive impacts during repeated testing with the second impact stress (1.8 GPa) lower than the first one (3.5 GPa). The C-scan images taken at the depth of 3.0 mm below the impact surface illustrate the scenario after the first (a), second (b) and third (c) impact, for which the applied impact stress equaled 3.5, 1.8 and 3.5 GPa, respectively.

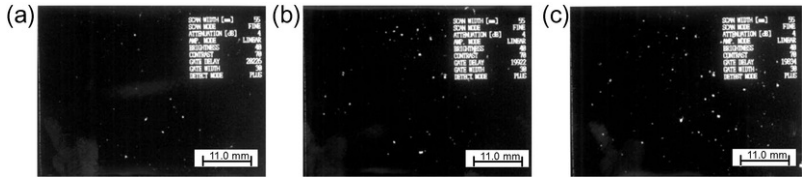

Fig. 6 The variation of spall-damage in commercially pure iron (sample No. N17) induced by consecutive impacts during repeated testing with the second impact stress (2.4 GPa) lower than the first one (3.6 GPa). The C-scan images taken at the depth of 3.0 mm below the impact surface illustrate the scenario after the first (a), second (b) and third (c) impact, for which the applied impact stress equaled 3.6, 2.4 and 2.2 GPa, respectively.

Fig. 7 The optical micrograph of the vertical cross-section of commercially pure iron specimen (sample No. N7) that indicates spall-damage to consists mainly of cracks. The image was taken after the first impact stress of 3.2 GPa.

Indeed, when the stress of second and third impact is higher than the previous one (Fig. 4) the damage after the each impact increases. Interestingly, the development of the spall-damage was observed for all the evaluated depths (Figs. 5 and 6). This occurs systematically when the second impact stress is lower than the first one. Our conclusion applies to generated cracks, *i.e.*, the crack generated by the first impact (refer to Fig. 7) develops during the second one, despite its impact stress is lower, similarly to the test result for carbon steel [8]. Moreover, in a case when the third impact stress is slightly lower than the threshold spall stress, there is no difference in spall damage observed after the second and third impacts (Fig. 6). In order to detect the cracks growth, we applied the quantitative ultrasonic evaluation to these particular specimens.

4.3 Change in ultrasonic velocity, attenuation, backscattering intensity and amplitude spectrum

Our previous experiments [8] confirmed that the wave velocity measured for metals with a large number of voids or cracks is lower than this measured for defect-free materials. This was deduced from agreement between the results of the C-scan acoustic microscopy and conventional ultrasonic measurements (see Figs. 4–6 at first impact and Fig. 8). The output results from the ultrasonic wave scattering at voids or cracks, while the presence of defects enhances attenuation and backscattering intensity [8,16]. Certainly, this prompted us to use the amplitude spectrum of backwall echo (B1) as a new parameter, in addition to ultrasonic wave velocity, attenuation (amplitude ratio, B2/B1) and backscattering intensity [8,9] to estimate the spall damage.

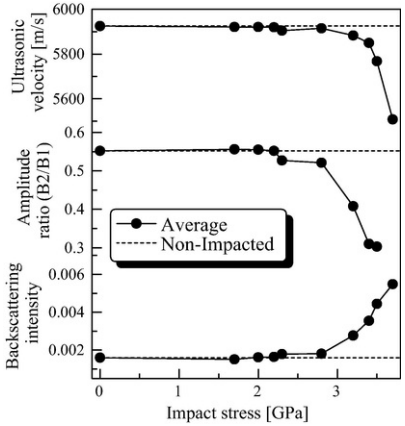

Fig. 8 Dependence of longitudinal wave (ultrasonic) velocity, amplitude ratio (equal B2/B1) and backscattering intensity on impact stress. The indicated ultrasonic variables were measured for the commercially pure iron after the first impact.

When the impact stress is lower than the threshold spall stress (approximately 2.3 GPa), the wave velocity, amplitude ratio, backscattering intensity and the amplitude spectrum are the same as for the non-impacted plates, as evident in Figs. 8 and 9. Indeed, even in the case of non-impacted plates, the amplitude ratio is less than unity (B2/B1 < 1) because of geometrical spreading of the ultrasonic beam. Moreover, the higher the impact stress (when it certainly exceeds the threshold spall stress) the lower is the velocity and the amplitude ratio, while the backscattering intensity increases with impact stress (Fig. 8). In the case of amplitude spectrum of the reflected wave (B1), the high frequency component attenuates markedly with an increase in the impact stress (Fig. 9). These observations prove the ultrasonic characteristics – such as the wave velocity, amplitude ratio, backscattering intensity and amplitude spectrum – serve as a proper quantitative evaluation of the spall-damage.

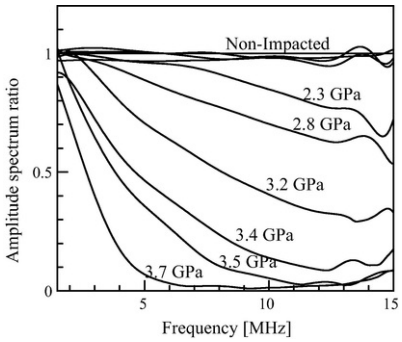

Fig. 9 Dependence of amplitude spectrum of backwall echo (B1) on impact stress. The indicated spectrum ratio was measured for the commercially pure iron after the first impact.

The measurement of the pertinent ultrasonic parameters was carried out for samples that were exposed to the repeated impact (*e.g.*, No. 17, the third impact stress is slightly lower than the threshold spall stress). As discussed in the preceding section, the acoustic images recorded for this particular sample do not provide sufficient information about the development of spall damage (see Fig. 6). However, the marked difference detected between velocities, amplitude ratios, backscattering intensity and amplitude spectrum recorded after the first, second and third impact (the values measured after the each impact changes in comparison with the previous one, see Figs. 10 and 11) make a ground to contend that spall damage increased during subsequent impact-events. This speaks in favor of the ultrasonic method we used to estimate the spall damage variation due to multiple impacts.

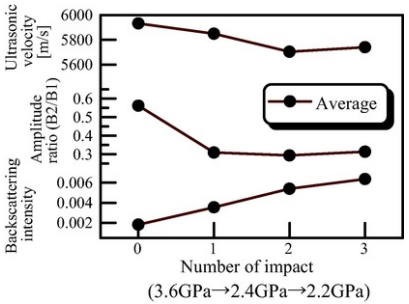

Fig. 10 Changes of ultrasonic velocity, amplitude ratio and backscattering intensity during the repeated impact test. The data correspond to C-scan images displayed in Fig. 6.

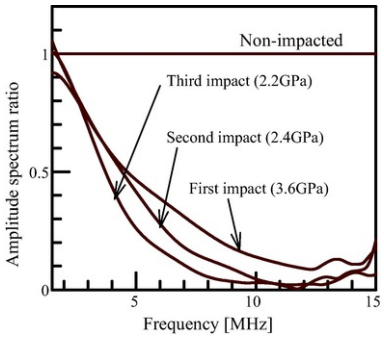

Fig. 11 Changes of amplitude spectrum during the repeated impact test. The data correspond to C-scan images displayed in Fig. 6.

5 Conclusions

The accumulation of the spall damage generated in commercially-pure iron during repeated plate impact testing was evaluated by means of the nondestructive, ultrasonic method. We successfully used the C-scan images and the amplitude-measurements for spectrum of the reflected waves (ultrasonic velocity, attenuation and backscattering intensity) to conclude on the introduced spall-damage and its development along the sequence of consecutive

impacts.

The cracks generated by the impact were found to extend during consecutive impacts. The damage recorded in C-scan images was found consistent with what we concluded from our measurements of ultrasonic velocity, attenuation, backscattering intensity and amplitude spectrum (details in Section 4.3). The evolution of the spall damage under repeated impacts can be monitored by the proposed set of ultrasonic measurements. This approach provides an effective means for nondestructive evaluation of spall-damage in metals and the mechanisms of its development during repeated impact tests.

References

[1] L. Davison and R.A. Graham, Shock compression of solids, *Phys. Rep.* **55** (4), 1979, 255–379.

[2] M.A. Meyers and C.T. Aimone, Dynamic fracture (spalling) of metals, *Progr. Mater. Sci.* **28**, 1983, 1–96.

[3] D.R. Curran, L. Seaman and D.A. Shockey, Dynamic failure of solids, *Phys. Rep.* **147** (5-6), 1987, 253–388.

[4] R.S. Gilmore, K.C. Tam, J.D. Young and D.R. Howard, Acoustic microscopy 10 to 100 MHz for industrial applications, *Philos. Trans. R Soc. London* **A320**, 1986, 215–235.

[5] Y. Ogura, T. Miyajima, H. Kino and I. Ishikawa, Identification and sizing technique of voids in LSI package by scanning acoustic tomography, *Adv. Electr. Pack. (ASME)* 1992, 973–976.

[6] B. Tittmann, C. Miyasaka, H. Kasano, Ultrasonic measurements of the elastic properties of impacted laminate composites, in: Proc. ECNDT 2006, Th.4.7.4.

[7] K. Kawashima, Ultrasonic nondestructive characterization of materials, *Trans. JSME-A* **67** (655), 2001, 370–377.

[8] N. Nishimura, K. Murase, T. Ito and R. Nowak, Ultrasonic evaluation of spall damage accumulation in aluminum and steel subjected to repeated impact, *Int. J. Impact Eng.* **38** (4), 2011, 152–161.

[9] N. Nishimura, K. Murase, T. Ito, T. Watanabe and R. Nowak, Ultrasonic detection of spall damage induced by low-velocity repeated impact, *Cent. Eur. J. Eng.* **2** (4), 2012, 650–655.

[10] Y. Oved and G.E. Luttwak, Shock wave propagation in layered composites, *J. Comp. Mater.* **12**, 1978, 84–96.

[11] T. Hayashi, Y. Tanaka, editors, Impact Engineering, Nikkan Kogyo Shimbun Ltd., 1988, pp. 6–15, pp. 105–108.

[12] J.A. Zukas, (Ed), *High Velocity Impact Dynamics, A Wiley-Interscience Publication,* 1990, John Wiley & Sons, INC, 20.

[13] M. Takada, M. Haccho, M. Hayashi and F. Uchino, Internal observation by acoustic microscope, *Opt. Electro-Opt. Eng. Contact* **27** (4), 1989, 212–219.

[14] G.S. Kino, Acoustic Waves: Devices, Imaging, and Analog Signal Processing, 1987, Prentice-Hall, pp. 182.

[15] K. Kawashima and I. Fujii, Digital measurement of ultrasonic velocity, *Rev. Prog. QNDE* **14**, 1995, 203–209.

[16] K. Kawashima, J. Okada, K. Nawa and N. Nishimura, Evaluation of minute cracks generated by spallation with nonlinear ultrasonic measurement, *Rev. Prog. QNDE* **20**, 2001, 1283–1289.

Queries and Answers

Query: Your article is registered as belonging to the Special Issue/Collection entitled “ULTRAS_materials science”. If this is NOT correct and your article is a regular item or belongs to a different Special Issue please contact s.nataraj@elsevier.com immediately prior to returning your corrections.
Answer: Our manuscript was registered to the special Issue "ULTRAS_materials science".

Query: The author names have been tagged as given names and surnames (surnames are highlighted in teal color). Please confirm if they have been identified correctly.
Answer: We confirmed our name.

Query: Please check the layout of Tables 1 and 2, and correct if necessary.
Answer: We do not need to correct them.